

Cryoaerogels and Cryohydrogels as Efficient Electrocatalysts

Dennis Müller, Dániel Zámbo, Dirk Dorfs,* and Nadja C. Bigall

Additive-free cryoaerogel coatings from noble metal nanoparticles are prepared and electrochemically investigated. By using liquid nitrogen or isopentane as cooling medium, two different superstructures are created for each type of noble metal nanoparticle. These materials (made from the same amount of particles) have superior morphological and catalytic properties as compared to simply immobilized, densely packed nanoparticles. The morphology of all materials is investigated with scanning electron microscopy (SEM). Electrochemically active surface areas (ECSAs) are calculated from cyclic voltammetry measurements. The catalytic activity is studied for the ethanol oxidation reaction (EOR). Both are found to be increased for superstructured materials prepared by cryoaerogelation. Furthermore, cryoaerogels with cellular to dendritic structure that arise from freezing with isopentane show the best catalytic performance and highest ECSA. Moreover, as a new class of materials, cryohydrogels are created for the first time by thawing flash-frozen nanoparticle solutions. Structure and morphology of these materials match with the corresponding types of cryoaerogels and are confirmed via SEM. Even the catalytic activity in EOR is in accordance with the results from cryoaerogel coatings. As a proof of concept, this approach offers a novel platform towards the easier and faster production of cryogelated materials for wet-chemical applications.

are fabricated by targeted destabilization of colloidal solutions and subsequent supercritical drying of the formed hydrogels, the recently discovered cryoaerogels are prepared following a straightforward freeze-drying method.

In the standard cryoaerogelation procedure, highly concentrated, colloidal nanoparticles in aqueous solution are flash-frozen by injecting or dipping into liquid nitrogen. With the high temperature gradient, a sudden crystallization of the solvent triggers the formation of small ice crystallites. The nanoparticles are excluded from the growing ice front and pushed close together into the space between the crystals. By using high nanoparticle concentrations (at least 0.1 vol%) the interstices of the formed ice-template are completely filled, the particles interconnect with each other and form sheet-like structures providing sufficient mechanical stability. After solidification, in order to avoid any capillary forces that would occur during conventional drying techniques

under ambient conditions, the ice-template is removed by lyophilization (freeze-drying). Thus, a 3D aerogel network with open pores and high surface areas is obtained.^[1] A scheme for the formation of this network is shown in **Figure 1**.

By fulfilling the above-mentioned criteria, the shape of the resulting cryoaerogel corresponds to the shape of the frozen colloid that plays important role in the stability of the structure. In contrast to other gelation techniques, this offers an opportunity to prepare aerogel materials with defined shapes by the use of molds or to directly create thin aerogel coatings by applying the nanoparticle solutions on substrates upon freezing.

While other cryo-based procedures for the production of porous materials are limited to substance-specific components (such as cryogelation for polymers), the cryoaerogelation technique can be used for all conceivable nanoparticle systems in aqueous solution. For example, cryoaerogels have already been produced from precious metals, metal oxides, and semiconductors.^[1]


Recently, the impact of different freezing parameters on the resulting cryoaerogel material has been investigated.^[6] In this context, it was shown that the freezing speed and thus the ice-template crystallization can be significantly influenced by the use of different freezing media or temperatures. In detail, by dipping a sample with room temperature into liquid nitrogen, the Leidenfrost effect leads to a bubble wrap of gaseous nitrogen around the sample. This causes lower heat conductivity, slower freezing of the sample, lamellar growth of the ice-template and thus a lamellar shape of the resulting aerogel material. In

1. Introduction

Since their first report in 2016,^[1] cryoaerogels from preformed nanoparticles are studied intensively due to their unique properties such as their high specific surface area and open-pore structure.^[2–6] However, in contrast to conventional nanocrystal aerogels,^[7] which

D. Müller, Dr. D. Zámbo, Prof. D. Dorfs, Prof. N. C. Bigall
Institute of Physical Chemistry and Electrochemistry
Leibniz Universität Hannover
Callinstraße 3A, 30167 Hannover, Germany
E-mail: dirk.dorfs@pci.uni-hannover.de

D. Müller, Dr. D. Zámbo, Prof. D. Dorfs, Prof. N. C. Bigall
Laboratory for Nano and Quantum Engineering
Leibniz Universität Hannover
Schneiderberg 39, 30167 Hannover, Germany
Prof. D. Dorfs, Prof. N. C. Bigall
Cluster of Excellence PhoenixD
Photonics, Optics and Engineering-Innovation Across Disciplines
30167 Hannover, Germany

 The ORCID identification number(s) for the author(s) of this article can be found under <https://doi.org/10.1002/sml.202007908>.

© 2021 The Authors. Small published by Wiley-VCH GmbH. This is an open access article under the terms of the Creative Commons Attribution-NonCommercial License, which permits use, distribution and reproduction in any medium, provided the original work is properly cited and is not used for commercial purposes.

DOI: 10.1002/sml.202007908

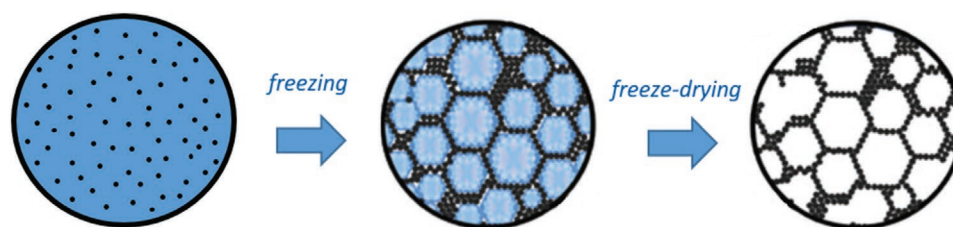


Figure 1. Basic principle of cryoaerogelation. From left to right: colloidal nanoparticle solution; frozen colloid; cryoaerogel.

contrast to that, by using freezing media with boiling points above room temperature (such as isopentane) the Leidenfrost effect is circumvented and the samples' freezing speed can be increased. As a result, different morphologies with significantly improved stability can be obtained. Thus, faster freezing leads to the formation of cellular or even dendritic shaped ice-templates and aerogel materials.^[6]

Since cryoaerogelation is a physical method, it is suitable for all kinds of materials such as metal, metal oxide, or semiconductor nanoparticles. So far, successful application of cryoaerogels have been shown in the fields of heterogeneous catalysis^[2] and photoelectrochemical sensing.^[5]

In this work, we put our focus on the first electrocatalytic application of cryoaerogels and further cryohydrogels, which are prepared here for the first time. With special regard to the utilization of nanocrystals in low temperature fuel cells, the electrochemical oxidation of hydrogen and small organic molecules became part of intensive studies.^[8] Especially noble metals were found to show high performances in electrocatalysis due to their high catalytic activity and stability compared to other catalysts.^[9] On the other hand, scarcity and high cost of these elements limit the large-scale industrial utilization.^[10] To overcome these limitations, efforts have been made to optimize the efficiency of the catalytic material. Here, aerogels with their high porosity offer a way to maximize the materials surface area and thus improve their catalytic mass activity.

Since ethanol is relatively inexpensive, comparatively non-toxic, and environmentally friendly,^[11–12] in this context, often the ethanol oxidation reaction (EOR) as part of direct ethanol fuel cells (DEFCs) is investigated for noble metal aerogels.^[13–16] For that, especially thin films or coatings from these materials on electrodes are of special interest.^[17–19] These materials are mainly prepared by drop-casting (and subsequent drying) of a slurry on the electrode that is consisting of the aerogel, solvents, and a binding substance such as Nafion.^[20–23] However, the monolithic structure is destroyed by mixing the slurry beforehand, so that the resulting coating consists of smaller aerogel fragments, that are covered and connected by the binding material. By these means, the coating procedure leads to a significant loss in accessible surface area and hierarchically structured pore system, as compared to monolithic materials without additives.

In this work, we created cryoaerogels from noble metal nanoparticle solutions directly in the form of monolithic electrode coatings. The additive-free approach maximizes the accessible surface area of the coating and by renouncing a carbon support, the longtime stability against corrosion is improved.^[24]

By freezing the colloidal solution with different freezing media we created cryoaerogel coatings with different structures and investigated their performance in electrocatalytic EOR. We

focused on alkaline electrolytes, since electrocatalytic activity for oxidation of organic fuels was found to be larger compared to acidic media.^[25,26] In more detail, for the first time, we show that cryoaerogelated materials yield in better electrocatalytic performances compared to simply immobilized nanoparticles of the same kind and amount due to higher accessible surface areas. We further show that cellular to dendritic cryoaerogel structures, which arise from freezing with isopentane, increase the active surface area even more and thus the electrocatalytic performance compared to lamellar cryoaerogel structures that are created by freezing with liquid nitrogen as in the standard cryoaerogelation.^[1]

Beyond these findings, for the first time, we proved that the cryoaerogel superstructure already exists in the frozen state and can be transferred into a wet state by simple thawing even without lyophilization. In addition to electron microscopic examinations, we show that these new, so-called cryohydrogels yield in an equal electrocatalytic activity when compared to the respective cryoaerogels. This key fact offers a new, easier, and faster approach for the utilization of cryoaerogel materials in a wet-chemical environment.

2. Results and Discussion

2.1. Electrochemical Characterization of Cryoaerogel Superstructures

To investigate the electrocatalytic performance of noble metal cryoaerogels, we prepared different types of ITO glass-based electrode coatings from these nanocrystals. For this, we synthesized and concentrated gold, platinum, or palladium nanoparticles in aqueous solution and used the same volume/amount of particles for each coating, respectively. On the one hand, following the standard procedure, cryoaerogel coatings were prepared by freezing with liquid nitrogen (N_2) at $-196\text{ }^\circ\text{C}$, which led to lamellar shaped superstructures. On the other hand, cellular to dendritic shaped cryoaerogel coatings were fabricated by freezing in isopentane at $-160\text{ }^\circ\text{C}$. For comparison to non-superstructured materials, we further immobilized the original nanoparticles by simple drop-casting and drying of the colloidal solution at ambient conditions. In this context, **Figure 2** exemplarily shows photographs as well as images from scanning electron microscopy (SEM) for the respective coatings from gold nanoparticles. Comparable images for the coatings from platinum and palladium particles can be found in Figures S2 and S3, Supporting Information.

After preparation, the electrochemical behavior of respective coatings was analyzed for the first time. At first, cyclic voltammetry (CV) was performed in N_2 -saturated potassium hydroxide

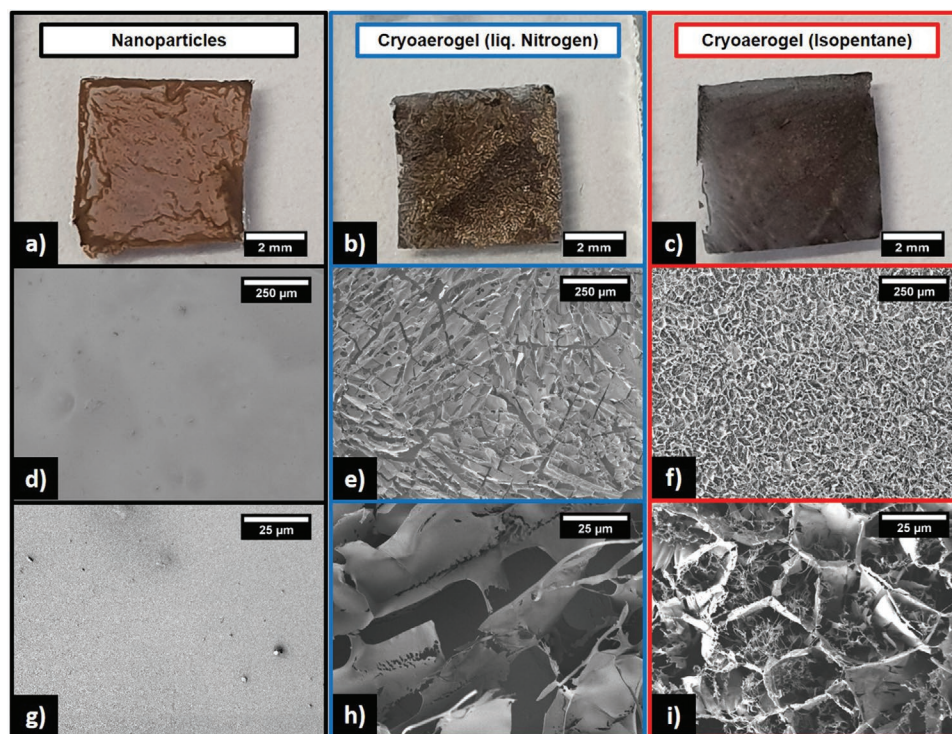


Figure 2. a–c) Photographs and d–i) SEM images of electrode coatings from gold nanoparticles. Left/black: drop-casted and dried nanoparticles. Middle/blue: Cryoerogel frozen with liquid N₂ at –196 °C. Right/red: Cryoerogel frozen with isopentane at –160 °C.

solution (KOH, 1 M). Obtained CV curves for all noble metal coatings are shown in **Figure 3a–c**.

To determine the electrochemical active surface areas (ECSAs), the charge for the reduction of the metal oxide was calculated by integrating the respective region in the reverse scan of the CV curves. Afterwards, the ECSAs were calculated based on Equation (1).

$$ECSA = \frac{\int IdU}{Q \cdot v \cdot m} \quad (1)$$

where $\int IdU$ is the total charge necessary for the metal oxide reduction, v is the scan rate (0.05 V s⁻¹), and m is metal loading (g) on the electrode. Q is the conversion factor, commonly taken as 0.386 mC cm⁻² for gold,^[27] 0.420 mC cm⁻² for platinum,^[28] and 0.405 mC cm⁻² for palladium.^[29] The calculated ECSAs for all noble metal coatings are displayed in **Figure 3d**. It can be clearly seen that coatings from simply drop-casted and dried nanoparticle solutions (black) show the smallest accessible, active surface area (10.5–12 m² g⁻¹), which was expected due to their flat and non-superstructured nature. In contrast, standard cryoerogels frozen with liquid N₂ (blue) and with the same amount of noble metal exhibit higher ECSAs (13.5–14.5 m² g⁻¹) which can be explained by their lamellar shaped superstructure. Additionally, cellular to dendritic shaped cryoerogels that were frozen with isopentane (red) were found to have even higher ECSAs (20–23 m² g⁻¹). Moreover, when comparing all tested noble metals, ECSAs are very similar for the same type of coating technique, which further proves the versatility of the cryoerogelation. Slight deviations

can be explained by different particle sizes and heat conductivities of the noble metals.

Additionally, for platinum coatings ECSAs were determined for the hydrogen underpotential deposition in the range of –0.8 to –0.5 V in the forward scan of the CV curves. The conversion factor for this process is commonly taken as 0.210 mC cm⁻² for platinum.^[30] Again, ECSAs were calculated by Equation (1). Here, the same trend was observed for coatings with different morphologies: Densely-packed nanoparticle coatings have the smallest accessible, active surface area (6.9 m² g⁻¹), whereas lamellar shaped cryoerogels exhibit higher ECSAs (8 m² g⁻¹). Again, cellular shaped cryoerogels show an even higher accessible surface area (8.7 m² g⁻¹).

Besides the electrochemically active surface area, the electrocatalytic performance of cryoerogels in the EOR was investigated for the first time. For this, cyclic voltammetry was performed in N₂-saturated KOH solution (1 M) containing ethanol (1 M). **Figure 4** displays obtained CV curves for all noble metal coatings, which were mass-normalized by the applied amount of noble metal. The amount was measured via inductively coupled plasma optical emission spectroscopy (ICP-OES). Afterwards, respective mass activities for EOR of each coating were identified from oxidation peaks in the forward scan. These are compared in **Figure 5a** for all coatings of all tested noble metals. Additionally, the ECSA-normalized activities are compared in **Figure 5b**.

In accordance with measured ECSAs, the number of accessible active sites and thus the performance of cryoerogel materials is greatly enhanced compared to immobilized nanoparticles of the same amount due to the superstructured

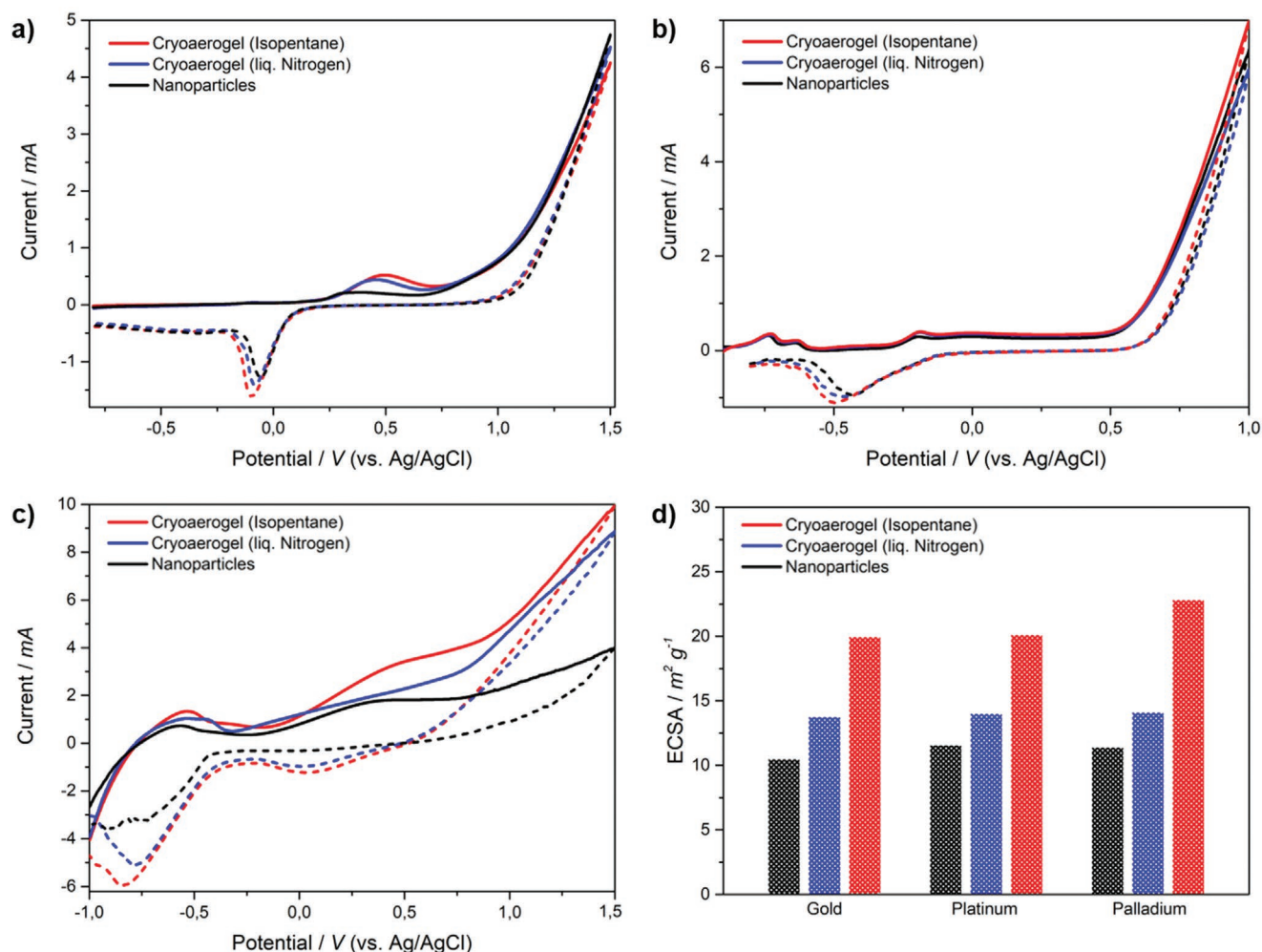


Figure 3. CVs of noble metal coatings in N₂-saturated KOH solution (1 M) at a scan rate of 50 mV s⁻¹. a) Gold. b) Platinum. c) Palladium. d) ECSAs compared for all noble metal coatings. Black: drop-casted and dried nanoparticles. Blue: Cryoaerogel frozen with liquid N₂ at -196 °C. Red: Cryoaerogel frozen with isopentane at -160 °C. Solid line: forward scan. Dashed line: reverse scan.

design. As well, cryoaerogels frozen with isopentane have significantly higher activities than those frozen with liquid N₂ (following the standard procedure). All tested noble metals show this behavior, which demonstrates that by control over the morphologically accessible surface areas can be enhanced and the electrochemical performance can be improved. Consistent with literature, the electrocatalytic activity thereby is generally element-specific, so that platinum materials show better performance in EOR than comparable gold materials. Over and above that, even higher activities can be achieved with palladium materials.^[31–32] This behavior can be seen clearly in the ECSA-normalized activities in Figure 5b. There, independent of their morphology coatings from the same material accordingly show nearly the same element-specific activity. This further indicates the same catalytic mechanism for all tested morphologies. Thus, the observed increase in electrocatalytic performance can be attributed to the materials' surface area and the increase of accessible active sites by the here presented gelation technique. The increase of catalytic activity by higher accessible surface areas was already confirmed in literature.^[14,27,33,34]

Further, a shift in the oxidation peak potential can be recognized in the forward scan for cryoaerogels frozen with isopentane (Figure 4). This overpotential can be explained by the diffusion controlled transport of ethanol species to the electrodes' active sites. In contrast to the lamellar shaped structure with large pores from standard cryoaerogels, isopentane-frozen cryoaerogels possess a cellular to dendritic structure with larger surface areas, a higher number of active sites, but a narrower pore-system, which leads to slower substance transport to reactive sites. In this regard, pore-size-dependent behavior of ECSA and substance transportation has already been shown for various gold nanostructures.^[35]

After all, for the first time, we were able to show catalytic activities of cryoaerogels and to further increase this activity by controlling the freezing parameters and creating defined morphologies with enhanced accessible surface area. The observed activities for cellular-shaped cryoaerogels (266 mA mg⁻¹ for gold, 988 mA mg⁻¹ for platinum, and 1538 mA mg⁻¹ for palladium) are comparable to those of other state-of-the-art noble metal nanomaterials and even partially exceed them. Dendritic gold

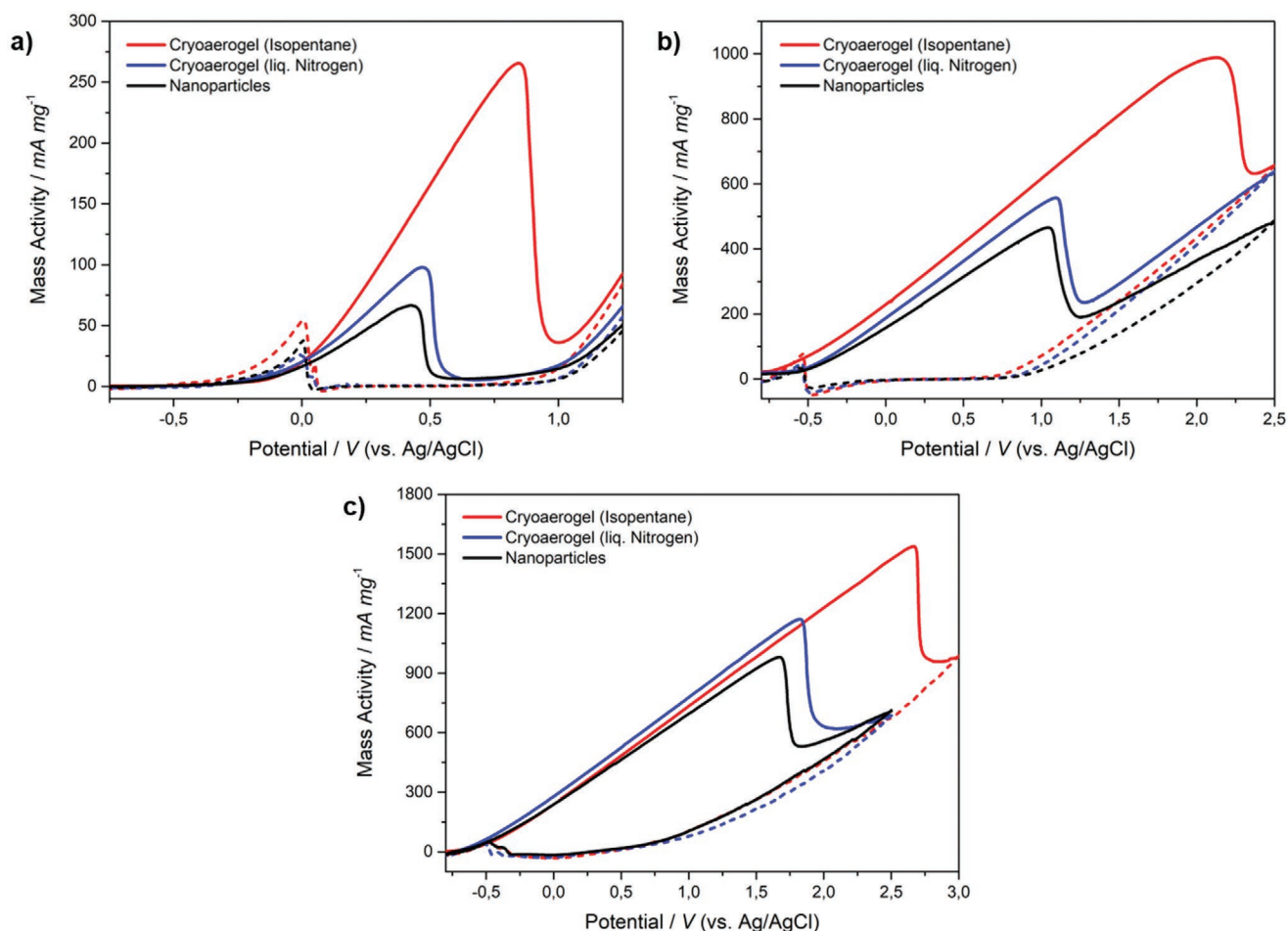


Figure 4. Mass-normalized CVs of gold coatings in N_2 -saturated KOH solution (1 M) containing ethanol (1 M) at a scan rate of 50 mV s^{-1} . a) Gold. b) Platinum. c) Palladium. Black: drop-casted and dried nanoparticles. Blue: Cryoaerogel frozen with liquid N_2 at -196°C . Red: Cryoaerogel frozen with isopentane at -160°C . Solid line: forward scan. Dashed line: reverse scan.

nanostructures for example showed an activity of 137 mA mg^{-1} in EOR, whereas polycrystal-gold showed 22 mA mg^{-1} .^[27] In the case of platinum, hollow nanosphere materials showed a comparable activity of 1000 mA mg^{-1} . Also, the

ECSA-normalized activity was of similar extent (48 mA cm^{-2}).^[14] For palladium, nanowire materials showed an EOR activity of $\approx 2000 \text{ mA mg}^{-1}$,^[36] and with specially tuned palladium aerogels already up to 7800 mA mg^{-1} have been observed.^[20] Compared

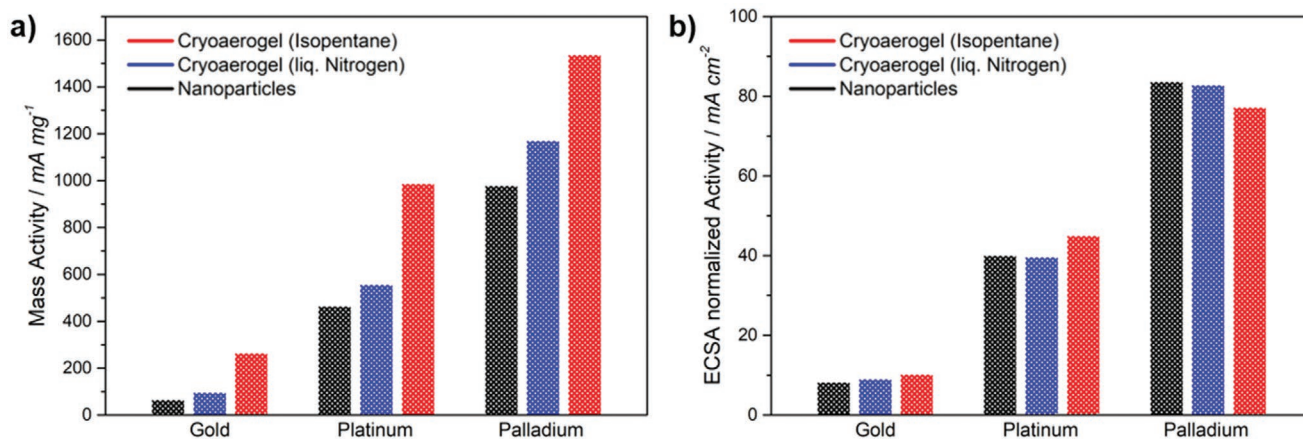


Figure 5. a) Mass-normalized and b) ECSA-normalized activities in EOR compared for respective gold, platinum, and palladium coatings. Black: drop-casted and dried nanoparticles. Blue: Cryoaerogel frozen with liquid N_2 at -196°C . Red: Cryoaerogel frozen with isopentane at -160°C .

with that, for conventional palladium catalysts, that are carbon-supported, only 40–60 mA mg⁻¹ were observed.^[37,38] This comparison clearly shows that the here presented materials based on monometallic, spherical particles can compete with state of the art catalysts. As already shown in literature,^[1] they might easily be extended to more sophisticated nanoparticle building blocks such as cubic, hollow, or alloy particles, which are expected to further enhance the catalytic activity of cryoaerogels.

2.2. Cryohydrogels

For applications in wet-chemical environment, cryoaerogel materials have to be transferred into a wet state. However, rewetting has to be very gentle due to possible destruction of the filigree gel network. Now, instead of freeze-drying and rewetting of as-prepared cryoaerogels, for the first time ever, we prepared so-called cryohydrogel materials just by the thawing of flash-frozen, highly concentrated colloids. By doing this, hours to days of production time can be saved and the process can also be simplified. And above all, the opportunity is offered to store flash-frozen samples in the frozen state until utilization and to gently thaw them in the wet-chemical environment right where they are used. Further, by keeping the colloid in the frozen state for a long enough time (≈ 24 h) before thawing is initiated, improved stability of the resulting gel materials is achieved.^[6] In this work, flash-frozen coatings from highly concentrated gold nanoparticle solutions were transferred into electrochemical cells and gently thawed inside of electrolyte solution. To shed light on the effect of morphology, both freezing techniques were applied (freezing with liquid N₂ at -196 °C and freezing with isopentane at -160 °C). Afterwards, we carried out the same electrocatalytic investigation for these cryohydrogels as for comparable cryoaerogel coatings (see above). The mass-normalized CV curves for the electrocatalytic EOR performance are shown in **Figure 6** and directly compared to those of rewetted cryoaerogels from **Figure 4a**.

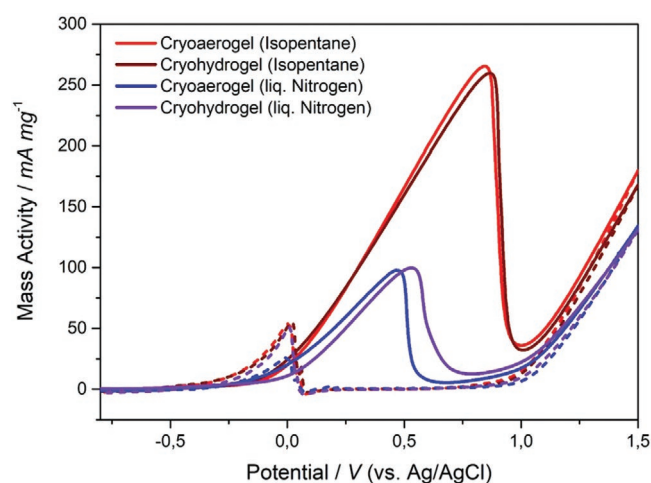


Figure 6. Mass-normalized CVs of gold cryoaerogels and cryohydrogels in N₂-saturated KOH solution (1 M) containing ethanol (1 M) at scan rate of 50 mV s⁻¹. Blue: Cryoaerogel and purple: Cryohydrogel frozen with liquid N₂ at -196 °C. Red: Cryoaerogel and brown: Cryohydrogel frozen with isopentane at -160 °C. Solid line: forward scan. Dashed line: reverse scan.

It can be seen that cryohydrogel coatings perform with the same activity as the rewetted cryoaerogel coatings. The similarity occurs for both superstructures frozen with liquid N₂ and frozen with isopentane and can be observed for respective coatings from platinum or palladium as well (see **Figure S4**, Supporting Information). Same activity, there, indicates the same amount of active sites and thus is the first evidence that thawed cryohydrogels exhibit the same surface area and microstructure as the freeze-dried (and rewetted) cryoaerogels.

For further evidence, we analyzed respective microstructures of these coatings by means of electron microscopy. Resulting SEM images from gold coatings frozen with liquid N₂ are presented in **Figure 7**.

On one hand, the typical, lamellar shaped structure of freeze-dried cryoaerogel coatings from the standard procedure is shown. On the other hand, we produced cryohydrogels by conventional drying of coatings under ambient conditions. As it can be seen from the SEM images, large parts of the lamellar structure collapsed due to the capillary forces acting during the drying process. Though, parts of a superstructured network are still recognizable, which indicates the existence of the cryoaerogel structure prior to conventional drying.

Finally, cryohydrogels were produced by gentle thawing inside aqueous solution. Afterwards, for being able to analyze with SEM, the cryohydrogels pore solution was carefully and gradually exchanged to dry acetone. Finally, these samples were supercritically dried and analyzed with electron microscopy. Here, from resulting SEM images, we identified the (basically) same lamellar shaped structure as from freeze-dried cryoaerogels. Comparable SEM images of cryoaerogel, -hydrogel, and -xerogel coatings frozen with isopentane are shown in **Figure S5**, Supporting Information. There, the same structural effects can be observed, too. As an important consequence, for the first time we were able to show that cryoaerogelated superstructures are already completely formed in the frozen state (before freeze-drying) and therefore can be simply transferred into the wet state by thawing, when they are kept in the frozen state for long enough (≈ 24 h) before the thawing is initiated.

In this context, the Eychmüller group recently showed the possibility to create noble metal nanoparticle gels induced by a freeze-thaw process.^[39] However, their method is based on ligand-free nanoparticle solutions and due to the necessarily low concentration no monolithic gel is created during freezing but smaller segments, that need to sediment and further aggregate after thawing. In contrast to that, the cryohydrogelation method presented in this work requires nanoparticles protected by ligands, but with sufficiently high concentration, we are able to create monolithic structures directly. Furthermore, defined shapes and additive-free coatings can be specifically manufactured by molding the nanoparticle solution before freezing.

Referring the results from structure elucidation to the electrocatalytic investigation of cryohydrogels (**Figure 4**), now, as expected, the observed similar catalytic activities can be ascribed to the same amount of active sites due to the confirmed identical microstructures of respective cryoaerogel and cryohydrogel coatings.

Lastly, supplementary to coatings in the form of quasi-2D thin films, we further verified the structure and existence of cryohydrogels for 3D, substrate-free materials too. Therefore, we used the same nanoparticle solution as for the coating and

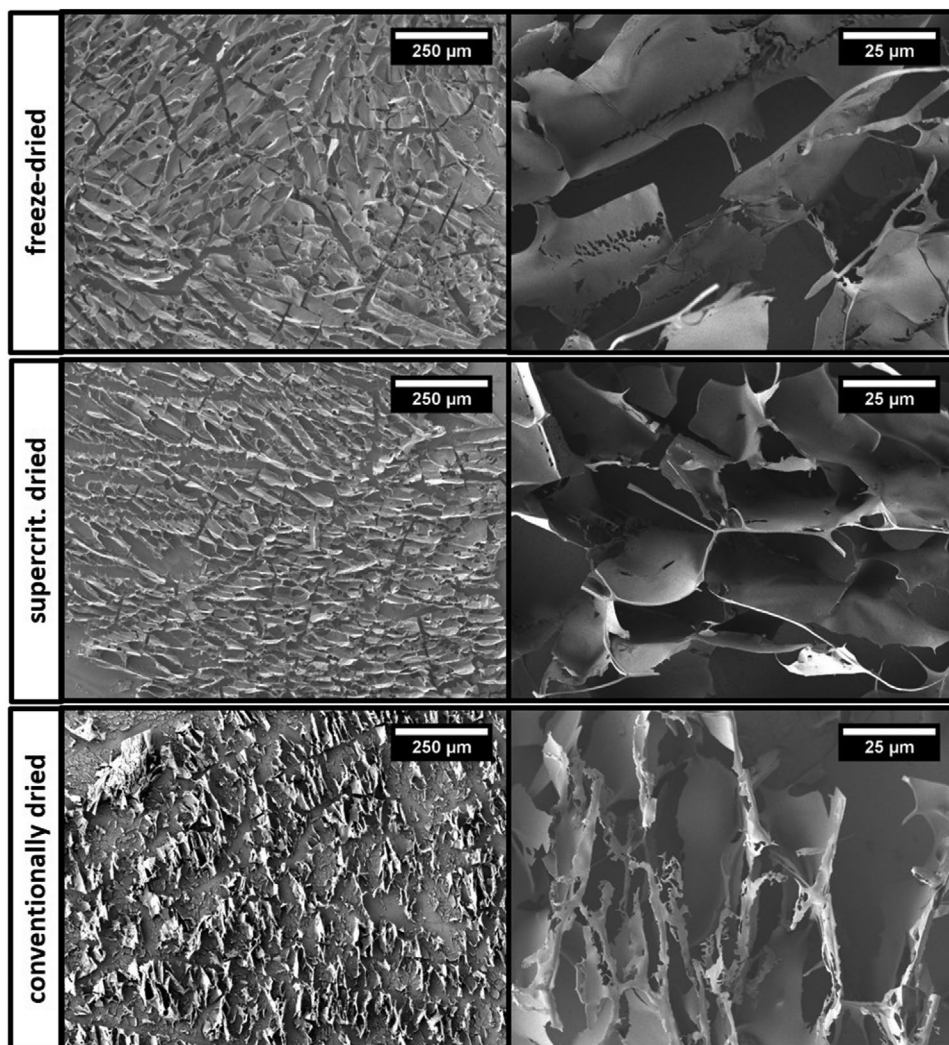


Figure 7. SEM images from freeze-dried cryo-aerogels (top), thawed and supercritically dried cryohydrogels (middle), and conventionally dried cryoxerogels (bottom) after flash-freezing of coatings from gold nanoparticle solution in liquid N₂ at −196 °C.

injected it into the respective freezing medium. Afterwards, as for the coated cryohydrogels, the samples were placed and thawed gently inside of aqueous solution, before exchanging the solvent with dry acetone. Finally, the gel materials were supercritically dried and investigated with electron microscopy. **Figure 8** displays the obtained SEM images for materials frozen with liquid N₂ at −196 °C as well as isopentane at −160 °C.

As we have recently shown, self-standing gels frozen with liquid N₂ consist of bigger sheets and large pores due to the slow freezing rate, whereas freezing with isopentane leads to higher freezing rates and thus finer structures with small pores.^[6] In accordance with this, the cryo-aerogelated superstructure can be preserved for the thawed and supercritically dried cryohydrogels in the same way like for the thin films.

3. Conclusion

In the first part of this study, we applied pure noble metal cryo-aerogels for the first time as efficient electrocatalysts in EOR

and thereby further enhanced the performance by fine-tuning their macroscopic superstructure. In detail, additive-free cryo-aerogel coatings with different morphologies were prepared via cryo-aerogelation of noble metal nanoparticles (gold, platinum, or palladium). On one hand, cryo-aerogel coatings with lamellar shape were created using liquid N₂ (at −196 °C) as freezing medium. These materials were found to show both, higher ECSA (121–131%) and improved electrocatalytic performance in EOR (120–147%) compared to non-structured, densely packed, drop-casted particles. On the other hand, isopentane (at −160 °C) was used as freezing medium to fabricate cryo-aerogel coatings with cellular/dendritic structure. By doing this, significantly higher ECSA (170–200%) and catalytic activity in EOR (157–400%) could be achieved. In future research, the activity may be further improved by known alloying strategies^[40–43] and by employment of nanoparticles or building blocks with different morphology and thus number of active sites.^[14,44–46]

In the second part of the article, we prepared a new type of material, the so-called cryohydrogels, by the thawing of flash-frozen, highly-concentrated, colloidal solutions. We were able

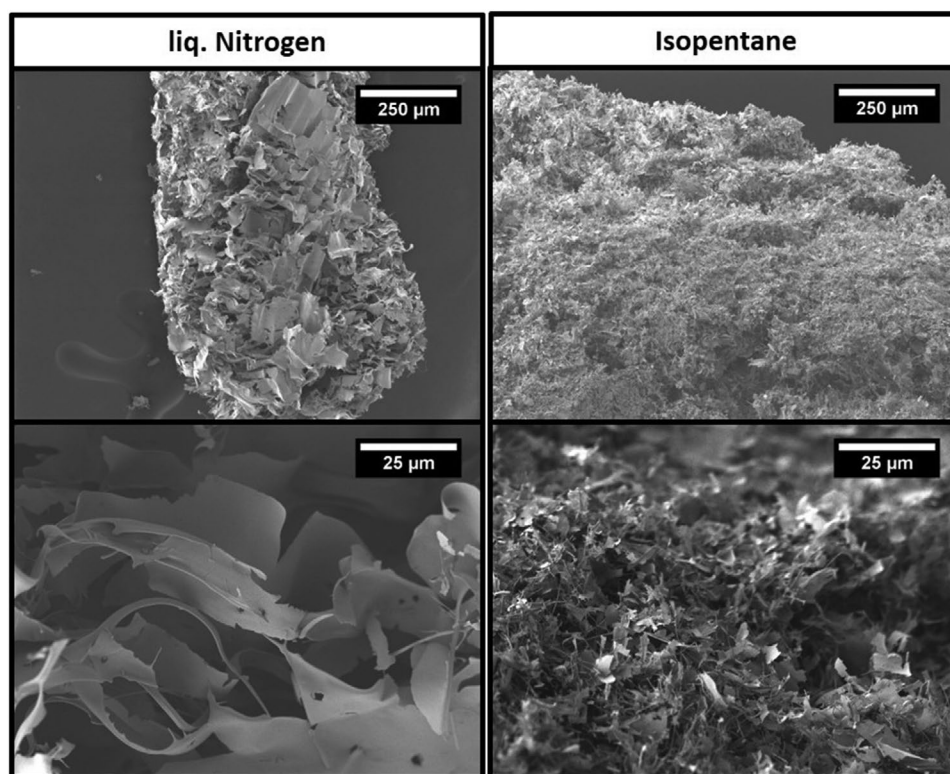


Figure 8. SEM images from substrate-free gold cryohydrogels after flash-freezing in liquid N₂ at −196 °C (left) or isopentane at −160 °C (right), subsequent thawing and supercritical drying.

to show, that the thawed materials exhibit the same superstructure as the corresponding type of cryoaerogel which is not thawed, but freeze-dried. In reverse, this proves the existence of the gel structure of cryoaerogels in the frozen state (already after flash-freezing even without freeze-drying). We were able to produce and confirm the morphology of these materials for thin films in the form of 2D coatings as well as for 3D, substrate-free gels. Furthermore, when applied in EOR, we found that the new cryohydrogels exhibit as high electrocatalytic activity as the re-wetted cryoaerogels. This additionally indicates the same morphology for both materials. As a conclusion, with our novel method cryogelated superstructures for wet-chemical applications can be received both faster and less complicatedly. Due to the structural diversity of such materials, the additive-free approach, and the versatility of applicable particles, we expect great benefits in all kinds of wet-chemical applications.

4. Experimental Section

Solutions of Noble Metal Nanoparticles: These were synthesized following a previously reported method.^[1]

Gold: We used 29 mL of a 0.2 wt% tetrachloroaurate (III) trihydrate solution (ABCR, 99.0%) and filled it with distilled water (18 MΩ cm) to a total volume of 500 mL. Under continuous stirring 11.6 mL of a 1 wt% trisodium citrate solution were added. Thirty seconds later, 5.8 mL of 0.17 wt% ice-cold sodium borohydride solution were injected whereupon the color of the solution turned from yellow to wine red. The reaction is completed within 1 min and the resulting colloid can be stored under ambient conditions (protected from sunlight).

Platinum: We used 36.2 mL of a 0.2 wt% dihydrogen hexachloroplatinate (IV) hexahydrate solution (Alfa Aesar) and filled it with distilled water (18 MΩ cm) to a total volume of 500 mL. Under continuous stirring this solution was boiled for 1 min at 100 °C, before 11.6 mL of a 1 wt% trisodium citrate solution was added. Thirty seconds later, 5.5 mL of 0.076 wt% ice-cold sodium borohydride solution was injected whereupon the color of the solution turned from yellow to dark brown. The reaction is completed within 1 min and the resulting colloid can be stored under ambient conditions.

Palladium: 0.0513 g palladium(II)chloride (Sigma Aldrich, 99.999%) was dissolved in 47.9 μL of 37 wt% hydrochloric acid (Sigma Aldrich) and filled with distilled water (18 MΩ cm) to a total volume of 500 mL. Under continuous stirring this solution was heated to 80 °C for 1 min, before 11.6 mL of a 1 wt% trisodium citrate solution was added. Thirty seconds later, 5.5 mL of 0.076 wt% ice-cold sodium borohydride solution was injected whereupon the color of the solution turned from yellow to dark brown. The reaction is completed within 1 min and the resulting colloid can be stored under ambient conditions.

Concentration of Nanoparticle Solutions: The volume of nanoparticle solutions was reduced from 500 to 50 mL by the use of a solvent resistant ultrafiltration cell (Merck Millipore), a 10 kDa polyethersulfon membrane (Sartorius Stedim) and a pressure of 5 bar. Afterwards, the remaining solutions were filled into centrifuge tubes with an inbuilt filter (Amicon Ultra-15, 10 kDa, Merck Millipore). At 4000 rcf for 5 to 8 min, the solutions were reduced stepwise to a volume of 0.25 mL. Finally, the solutions were washed three times. For this, solutions were mixed with 5 mL distilled water and reduced to 0.25 mL again by the use of a centrifuge filter.

Preparation of Substrates: For substrates, ITO-coated glass were cut into pieces of 1.5 × 1.0 cm and their surface was modified with (3-aminopropyl)triethoxysilane (APTMS). For this, the surface of the glass substrates was activated in the first step by immersing them in a mixture of 40 mL distilled water, 8 mL hydrogen peroxide (30%, Sigma Aldrich), and 8 mL ammonium hydroxide solution (25 wt%, Sigma

Aldrich). Under continuous stirring, the solution was heated to 50 °C for 30 min. Afterwards the activated glass substrates were rinsed with distilled water and isopropanol (Merck) and dried with compressed air. In a second step, the activated glass substrates were modified with APTMS. They were immersed in a solution of 0.15 mL APTMS (Acros) in 60 mL toluene (Sigma Aldrich) and heated to 70 °C for 2 h under continuous stirring. Afterwards, the modified substrates were rinsed with toluene and dried with compressed air.

Cryoaerogels: To prepare cryoaerogel coatings, defined square-shaped areas (0.5 × 0.5 cm) were masked on the modified glass substrates by the use of scotch tape. Afterwards, a total amount of 1 µL of the concentrated nanoparticle solution was applied to the substrate and distributed uniformly on the area to be coated. The samples were then flash-frozen by dipping in the respective freezing medium (liquid nitrogen at −196 °C or isopentane at −160 °C) for 10 min. Subsequently, the samples were freeze-dried in a lyophilizer (Christ Alpha 1–2 LD+) at 0.04 mbar for 18 h. To prepare substrate-free, monolithic cryoaerogels, a total amount of 50 µL of the concentrated nanoparticle solution was flash-frozen by being injecting directly into a vial with the cooling medium for 10 min before freeze-drying. All received cryoaerogels were stored under ambient conditions.

Cryohydrogels and Cryoxerogels: The samples were prepared in the same way as for the preparation of cryoaerogels (see above). Though, to gain cryoxerogels, the samples were dried under ambient conditions after flash-freezing. For the preparation of cryohydrogels, on the other hand, the flash-frozen samples were placed into aqueous solution for gentle thawing of the ice-template.

Supercritical Drying: Before supercritical drying, flash-frozen samples were placed into acetone at −20 °C. For the gentle thawing of the ice-template, the samples were then stored in a fridge at 5 °C over-night. Afterwards, samples were stored at room temperature for 3 days, meanwhile acetone was exchanged for three times. The completely washed acetogels (in anhydrous acetone) were finally dried inside of an E3100 critical point dryer from Quorum Technologies. Here, the acetone was washed out completely by flushing with liquid carbon dioxide (CO₂) and the samples were stored in the chamber overnight. Next day, the device was flushed with fresh liquid CO₂ and brought above the supercritical conditions (31.1 °C and 73.9 bar) by heating with a water bath circulator. To retrieve the aerogels, after 5 min, the device was vented very slowly and after reaching ambient pressure, the temperature was reduced back to room temperature.

Electrochemical Measurements: These were performed in a three-electrode set-up. Respective cryoaerogel and cryohydrogel coatings were used as the working electrode. A platinum wire was used as counter electrode and a silver/silver chloride (Ag/AgCl) electrode as a reference. For cyclic voltammetry we used potassium hydroxide (KOH) solution (1 M) and for EOR we used KOH (1 M) + ethanol (1 M) solution as electrolyte. The scan rate was 50 mV s^{−1} during all electrochemical measurements.

Scanning Electron Microscopy (SEM): For SEM, a JEOL JFM 6700F electron microscope was operated at 2 kV. Self-supported, monolithic cryoaerogels were placed onto adhesive carbon polymer pads. Substrates with cryoaerogel coatings were placed onto adhesive carbon polymer pads and glued with silver lacquer.

Inductively Coupled Plasma Optical Emission Spectrometry (ICP-OES): For analyzing the applied noble metal amount, each sample was dissolved in 2 mL aqua regia, which was prepared by mixing hydrochloric acid (37%, Fluka) and nitric acid (65%, Sigma Aldrich) in a ratio of 3:1. After 1 day, the solutions were filled up with nitric acid (4%) to a volume of 25 mL and measured with a 5110 ICP-OES from Agilent Technologies. For calibration solutions with defined concentrations (0, 0.5, 1.25, 2.5, 5, and 10 mg L^{−1}) were produced by the use of gold, platinum, or palladium standard solution (Fluka), respectively. Each sample was measured at three different wavelengths and each measurement was reproduced with three samples.

UV/Vis Absorbance Measurements: UV/Vis absorbance spectra of the nanoparticle solutions were recorded with a Dual-FL (HORIBA Jobin Yvon Inc.) inside of a 3 mL quartz cuvette (1 cm path length) at room temperature.

Dynamic Light Scattering: Particle size measurements were acquired with a Zetasizer Nano ZSP from Malvern Panalytical inside of a 3 mL disposable cuvette at room temperature.

Supporting Information

Supporting Information is available from the Wiley Online Library or from the author.

Acknowledgements

The project has in parts been funded by the Deutsche Forschungsgemeinschaft (DFG, German Research Foundation) under Germany's Excellence Strategy within the Cluster of Excellence PhoenixD (EXC 2122, Project ID 390833453). The authors also would like to acknowledge the DFG (grant agreement BI 1708/4-1 & DO 1580/5-1), the European Research Council (European Union's Horizon 2020 research and innovation program, grant agreement 714429), and the German Federal Ministry of Education and Research (BMBF) within the framework of the program NanoMatFutur (support code 03X5525) for financial support. D.M. is thankful for financial support from the Hannover School for Nanotechnology (hsn) and the Graduiertenakademie of the Leibniz Universität Hannover. The authors moreover thank Armin Feldhoff and Jürgen Caro for providing the SEM facility as well as the Institute for Inorganic Chemistry for providing the ICP-OES facility.

Open access funding enabled and organized by Projekt DEAL.

Conflict of Interest

The authors declare no conflict of interest.

Data Availability Statement

Research data are not shared.

Keywords

aerogel coatings, cryoaerogels, cryohydrogels, electrocatalysis, ethanol oxidation

Received: December 15, 2020

Revised: February 1, 2021

Published online: March 21, 2021

- [1] A. Freytag, S. Sánchez-Paradinas, S. Naskar, N. Wendt, M. Colombo, G. Pugliese, J. Poppe, C. Demirci, I. Kretschmer, D. W. Bahnemann, P. Behrens, N. C. Bigall, *Angew. Chem., Int. Ed.* **2016**, *55*, 1200.
- [2] A. Freytag, M. Colombo, N. C. Bigall, *Z. Phys. Chem.* **2017**, *231*, 63.
- [3] T. Kodanek, A. Freytag, A. Schlosser, S. Naskar, T. Härtling, D. Dorfs, N. C. Bigall, *Z. Phys. Chem.* **2018**, *232*, 1675.
- [4] A. Freytag, C. Günemann, S. Naskar, S. Hamid, F. Lübkeermann, D. Bahnemann, N. C. Bigall, *ACS Appl. Nano Mater.* **2018**, *1*, 6123.
- [5] A. Schlosser, L. C. Meyer, F. Lübkeermann, J. F. Miethe, N. C. Bigall, *Phys. Chem. Chem. Phys.* **2019**, *21*, 9002.
- [6] D. Müller, L. F. Klepzig, A. Schlosser, D. Dorfs, N. C. Bigall, submitted.
- [7] M. A. Aegerter, N. Leventis, M. M. Koebel, *Aerogels Handbook*, Springer, New York, NY **2011**.

- [8] M. Koper, A. Wieckowski, *Fuel Cell Catalysis: A Surface Science Approach*, John Wiley & Sons, Hoboken, NJ **2009**.
- [9] H.-J. Yin, J.-H. Zhou, Y.-W. Zhang, *Inorg. Chem. Front.* **2019**, *6*, 2582.
- [10] Y. Li, Y. Sun, Y. Qin, W. Zhang, L. Wang, M. Luo, H. Yang, S. Guo, *Adv. Energy Mater.* **2020**, *10*, 1903120.
- [11] K.-B. Ma, D.-H. Kwak, S.-B. Han, H.-S. Park, D.-H. Kim, J.-E. Won, S.-H. Kwon, M.-C. Kim, S.-H. Moon, K.-W. Park, *ACS Sustainable Chem. Eng.* **2018**, *6*, 7609.
- [12] E. A. Monyoncho, T. K. Woo, E. A. Baranova, *Electrochemistry: Volume 15*, Vol. 15, SPR - Electrochemistry, The Royal Society of Chemistry, London **2019**, pp. 1–57.
- [13] R. Du, J. Wang, R. Hübner, X. Fan, I. Senkovska, Y. Hu, S. Kaskel, A. Eychmüller, *Nat. Commun.* **2020**, *11*, 1590.
- [14] F.-M. Li, Y.-N. Zhai, Z.-Q. Wu, S.-N. Li, J.-M. Lee, *Adv. Mater. Interfaces* **2016**, *3*, 1600563.
- [15] B. Cai, A. Eychmüller, *Adv. Mater.* **2019**, *31*, 1804881.
- [16] A. S. Douk, H. Saravani, *ACS Omega* **2020**, *5*, 22031.
- [17] Q. Jiang, P. Xu, M. Sun, *J. Sep. Sci.* **2020**, *43*, 1323.
- [18] H. Budunoglu, A. Yildirim, M. O. Guler, M. Bayindir, *ACS Appl. Mater. Interfaces* **2011**, *3*, 539.
- [19] R. W. Pekala, J. C. Farmer, C. T. Alviso, T. D. Tran, S. T. Mayer, J. M. Miller, B. Dunn, *J. Non-Cryst. Solids* **1998**, *225*, 74.
- [20] W. Liu, A.-K. Herrmann, D. Geiger, L. Borchardt, F. Simon, S. Kaskel, N. Gaponik, A. Eychmüller, *Angew. Chem., Int. Ed.* **2012**, *51*, 5743.
- [21] W. Liu, A.-K. Herrmann, N. C. Bigall, P. Rodriguez, D. Wen, M. Oezaslan, T. J. Schmidt, N. Gaponik, A. Eychmüller, *Acc. Chem. Res.* **2015**, *48*, 154.
- [22] J. Mao, F.-F. Wu, W.-H. Shi, W.-X. Liu, X.-L. Xu, G.-F. Cai, Y.-W. Li, X.-H. Cao, *Chin. J. Polym. Sci.* **2019**, *38*, 514.
- [23] W. Liu, P. Rodriguez, L. Borchardt, A. Foelske, J. Yuan, A.-K. Herrmann, D. Geiger, Z. Zheng, S. Kaskel, N. Gaponik, R. Kötz, T. J. Schmidt, A. Eychmüller, *Angew. Chem., Int. Ed.* **2013**, *52*, 9849.
- [24] M. Georgi, B. Klemmed, A. Benad, A. Eychmüller, *Mater. Chem. Front.* **2019**, *3*, 1586.
- [25] J. S. Spendelow, A. Wieckowski, *Phys. Chem. Chem. Phys.* **2007**, *9*, 2654.
- [26] J. S. Spendelow, G. Q. Lu, P. J. A. Kenis, A. Wieckowski, *J. Electroanal. Chem.* **2004**, *568*, 215.
- [27] A. Zhang, Y. Chen, Z. Yang, S. Ma, Y. Huang, G. Richter, P. Schützendübe, C. Zhong, Z. Wang, *ACS Appl. Energy Mater.* **2020**, *3*, 336.
- [28] F. P. Lohmann-Richters, B. Abel, Á. Varga, *J. Mater. Chem. A* **2018**, *6*, 2700.
- [29] H. Lv, L. Sun, L. Zou, D. Xu, H. Yao, B. Liu, *Chem. Sci.* **2019**, *10*, 1986.
- [30] S. Trasatti, O. A. Petrii, *Pure Appl. Chem.* **1991**, *63*, 711.
- [31] L. Ma, D. Chu, R. Chen, *Int. J. Hydrogen Energy* **2012**, *37*, 11185.
- [32] J. Bai, D. Liu, J. Yang, Y. Chen, *ChemSusChem* **2019**, *12*, 2117.
- [33] S. Xiao, F. Xiao, Y. Hu, S. Yuan, S. Wang, L. Qian, Y. Liu, *Sci. Rep.* **2014**, *4*, 4370.
- [34] L. Nahar, A. A. Farghaly, R. J. A. Esteves, I. U. Arachchige, *Chem. Mater.* **2017**, *29*, 7704.
- [35] G. Hyun, T. Song, C. Ahn, Y. Ham, D. Cho, J. Oh, S. Jeon, *Proc. Natl. Acad. Sci. USA* **2020**, *117*, 5680.
- [36] V. Lesnyak, A. Wolf, A. Dubavik, L. Borchardt, S. V. Voitekhovich, N. Gaponik, S. Kaskel, A. Eychmüller, *J. Am. Chem. Soc.* **2011**, *133*, 13413.
- [37] H. Zhang, D. Wang, *Angew. Chem.* **2008**, *120*, 4048.
- [38] L. Xiao, L. Zhuang, Y. Liu, J. Lu, H. D. Abruna, *J. Am. Chem. Soc.* **2009**, *131*, 602.
- [39] R. Du, J.-O. Joswig, R. Hübner, L. Zhou, W. Wei, Y. Hu, A. Eychmüller, *Angew. Chem., Int. Ed.* **2020**, *59*, 8293.
- [40] C. Zhu, Q. Shi, S. Fu, J. Song, H. Xia, D. Du, Y. Lin, *Adv. Mater.* **2016**, *28*, 8779.
- [41] X. Tian, X. Zhao, Y.-Q. Su, L. Wang, H. Wang, D. Dang, B. Chi, H. Liu, E. J. M. Hensen, X. W. Lou, B. Y. Xia, *Science* **2019**, *366*, 850.
- [42] S.-H. Han, H.-M. Liu, P. Chen, J.-X. Jiang, Y. Chen, *Adv. Energy Mater.* **2018**, *8*, 1801326.
- [43] K. Eid, Y. H. Ahmad, H. Yu, Y. Li, X. Li, S. Y. AlQaradawi, H. Wang, L. Wang, *Nanoscale* **2017**, *9*, 18881.
- [44] J. Sheng, J. Kang, Z. Hu, Y. Yu, X.-Z. Fu, R. Sun, C.-P. Wong, *J. Mater. Chem. A* **2018**, *6*, 15789.
- [45] C. Li, M. Iqbal, B. Jiang, Z. Wang, J. Kim, A. K. Nanjundan, A. E. Whitten, K. Wood, Y. Yamauchi, *Chem. Sci.* **2019**, *10*, 4054.
- [46] D. Xu, H. Lv, H. Jin, Y. Liu, Y. Ma, M. Han, J. Bao, B. Liu, *J. Phys. Chem. Lett.* **2019**, *10*, 663.